Eurographics Symposium on Rendering - Experimental Ideas & Implementations (2017)
P. Sander and M. Zwicker (Editors)

Controlling and Sampling Visibility Information on the Image Plane

Christian Lessig

Otto-von-Guericke Universität Magdeburg

Abstract

Anti-aliasing on the image plane is a classic problems in computer graphics. While mip-mapping provides an efficient means to pre-filter texture information, no comparable technique exists for visibility. We address visibility-induced aliasing by exploiting that the Fourier transform of a discontinuity decays slowly only in the normal direction. Pre-filtering is thus only necessary in this direction and, after a coordinate transformation, the corresponding one dimensional problem can be solved analytically or tabulated. The resulting pre-filtered signal can be reconstructed exactly from pointwise samples and we derive corresponding sampling theorems that are tailored to the pre-filtering as well as a set of irregular sampling locations. We demonstrate our methodology for the classical Shannon-Nyquist setting but also for shift-invariant spaces where exact reconstruction kernels with significantly faster decay than the sinc-function are available. Our experimental results demonstrate that our pre-filtering is highly effective and that going beyond the Shannon-Nyquist setting reduces aliasing error further.

CCS Concepts

•***Computing methodologies*** → ***Visibility;***

1. Introduction

Since it was first observed that the "jaggies" in computer-generated images are a form of aliasing [Cro77], many approaches have been proposed to address the problem. To this date, however, anti-aliasing remains an active area of research (e.g. [RKLC*11, LA06, Res09]). To a large extent, this is because the pre-filtering that is required to reduce aliasing [Cro77, Cat78] is difficult to realize for visibility. In the following we will address this issue and provide an efficient means to regularize the visibility discontinuity. Together with sampling theorems that are tailored to the pre-filtering and an arbitrary but fixed irregular set of samples, this substantially reduces aliasing error.

Concretely, the problem we consider is the following. We assume that the image is represented by the pixel (or characteristic) basis so that the value I_{ij} of pixel P_{ij} is given by

$$I_{ij} = \int_{P_{ij}} I(x)\,dx \tag{1}$$

where $I(x)$ is the irradiance function on the image plane (or some other suitable intensity function). We are interested in obtaining an approximation $\tilde{I}_{ij}$ of I_{ij} from pointwise samples $I(\lambda_n)$ only, i.e.

$$I_{ij} \approx \tilde{I}_{ij} = \sum_n w_n I(\lambda_n) \tag{2}$$

where w_n are suitable weights. We will assume that the sample locations λ_n are confined to the pixel, i.e. $\lambda_n \in P_{ij}$, and λ_n, w_n are fixed but can be chosen, as it is for example the case on graphics hardware. We will furthermore assume that our geometry is described by polygons. Our objective is then to minimize the ℓ_p error

$$E = \Big(\sum_{ij} |I_{ij} - \tilde{I}_{ij}|^p \Big)^{1/p} \tag{3}$$

caused by visibility-induced aliasing for suitable $1 \leq p < \infty$.

The approximation $\tilde{I}_{ij}$ can be determined efficiently and reliably from a small number of pointwise samples $I(\lambda_n)$ when the irradiance signal is pre-filtered. While such pre-filtering is well understood when high frequencies are caused by textures [Wil83, Hec89], it is much more difficult for geometric discontinuities. To realize it in this case, we exploit that the Fourier transform of a discontinuity decays slowly only in the normal direction. This reduce the pre-filtering to a one dimensional task along the normal direction and, using an appropriate coordinate transformation, the corresponding convolution or projection can be solved analytically or precomputed. Since we determine a pixel value from samples, at runtime the regularized signal only needs to be evaluated pointwise, see Fig. 1 for an overview.

While the pre-filtered signal can in principle be reconstructed from its samples, the non-uniform locations commonly used in graphics are not compatible with Shannon's theorem. We will hence construct sampling theorems for non-uniform locations, for example those used on graphics hardware. These then directly yield the quadrature weights w_k for Eq. 2. Next to the classical setting of bandlimited functions we will derive sampling theorems also

for shift-invariant spaces [AG01] where, for suitable choices of the generator, reconstruction kernels with much faster decay than the sinc-function are available.

Our approach does not take perceptual questions into account, despite the importance of this aspect [Mit87, LA06]. Nonetheless, we feel that our approach does make a perceptual difference, as we demonstrate with preliminary experimental results in Sec. 4. These also show that moving beyond the Shannon-Nyquist setting can indeed improve the performance of sampling-based rendering.

2. Related Work

Since the literature on anti-aliasing is vast, we will focus in the following discussion on related work most relevant for our method.

Feibusch, Levoy, and Cook [FLC80] proposed to subdivide the overlap between a triangle and a pixel and then use a lookup table to approximate the integral with a given kernel. A lookup table was also used in later works such as those by Abram, Westover and Whitted [AW85] and Guenter and Tumblin [GT96]. By using the directionality of the Fourier transform we reduce visibility anti-aliasing to a one dimensional task that either has a closed form solution or is much more easily tabulated than the two or three dimensional functions used in previous work. The use of a sampling-based method also avoids the complex subdivision required in [FLC80, AW85].

Guenter and Tumblin [GT96] used Gaussian quadrature to solve integrals required for anti-aliasing and later Oulette and Fiume [OF01] systematically investigated the integration of discontinuous functions. We make this integration tractable by pre-filtering the discontinuity. Furthermore, instead of using pre-existing quadratures we construct custom ones that are adapted to the pre-filtering and a set of non-uniform locations. The computation of quadrature weights for anti-aliasing was recently investigated in [LA06] where a non-linear optimization problem was solved to obtain these. In contrast, we derive quadrature weights for arbitrary sampling locations using an analytical theory that only requires the solution of a simple linear system, although without taking perceptual aspects into account as in [LA06].

McCool [McC95] addressed aliasing by exploiting that the convolution of two splines is again a spline so that, when surface intensity and the image filter are represented this way, an accurate and efficient evaluation is possible. Our work employs shift-invariant spaces, which include splines, although our focus is on sampling based anti-aliasing, in contrast to the fully analytic approach explored by McCool. Manson and Schaefer [MS13] proposed the use of wavelets and their multi-resolution structure to solve the aliasing problem. This is not unlike our approach where we employ wavelet scaling functions to generate shift-invariant spaces. However, the implementation in [MS13] only uses Haar wavelets whereas for our work it is critical to have functions that are better localized in space and frequency.

Dippé and Wold [DW85] used Fourier theory to investigate how anti-aliasing on the image plane can be achieved using stochastic sampling [Coo86]. Mitchell [Mit87, MN88, Mit91] subsequently extended this work to include perceptual aspects. While we also base our work on Fourier theory, we exploit its directionality and localize it, which was not done in previous work. Frequency domain-inspired approaches have recently also played a prominent role in global illumination [DHS*05]. In particular, Ramamoorthi et al. [RAMN12] and Egan et al. [EHDR11] studied visibility information and its sampling in the Fourier domain. However, they did not address pre-filtering and only considered bandlimited functions.

An alternative to addressing the aliasing problem itself is to implement anti-aliasing as an post-processing step [Res09]. This is similar to recent work on noise reduction for Monte Carlo rendering, see [ZJL*15] for a survey.

3. Addressing the Aliasing Problem

After fixing some notation we develop in the following our line of attack on visibility-induced aliasing and discuss why the required pre-filtering is intrinsically only one dimensional. Afterwards we consider discuss how our methodology can be realized in the classical Shannon-Nyquist setting before turning to shift invariant spaces. We conclude the section with a discussion on how to chose the appropriate "capacity", e.g. bandlimit, of a function space for a given set of samples. An implementation of the discussed ideas is provided in the supplementary material and the reader should refer there for implementation aspects.

3.1. Preliminaries

The unitary Fourier transform $\hat{f}(\xi)$ of a function $f : \mathbb{R}^n \mapsto \mathbb{R}$ is

$$\hat{f}(\xi) = \int_{\mathbb{R}^n_x} f(x)\, e^{-2\pi i \langle \xi, x \rangle}\, dx \tag{4a}$$

with inverse transform

$$f(x) = \int_{\mathbb{R}^n_\xi} \hat{f}(\xi)\, e^{2\pi i \langle x, \xi \rangle}\, d\xi. \tag{4b}$$

The classical example for a sampling theorem is those by Shannon. It states that a B-bandlimited function $f : \mathbb{R}^n \to \mathbb{R}$, that is one satisfying

$$\operatorname{supp}(\hat{f}) \subset [-B, B]^n, \tag{5}$$

can be reconstructed from its pointwise samples $f(k/2B)$ at a B-dilated integer grid as

$$f(x) = \sum_{k \in \mathbb{Z}^n} f(k/2B)\, \operatorname{sinc}_B(x-k) \tag{6}$$

where $\operatorname{sinc}_B(x-k)$ is the B-dilated sinc-function in n dimensions (i.e. the n-fold tensor product of the one dimensional function).

3.2. Attacking Visibility-Induced Aliasing

An efficient and accurate approximation of the pixel value I_{ij} from a small number of pointwise values $I(\lambda_n)$ is possible when the irradiance signal $I(x)$ lies in (or sufficiently close) to a function space $\mathcal{H}$ that admits a sampling theorem with respect to the λ_n [LDF14]. $I(x)$ can then be represented using a sampling expansion with dual kernel functions $\tilde{k}_n(x)$ as

$$I(x) = \sum_n I(\lambda_n)\, \tilde{k}_n(x); \tag{7}$$

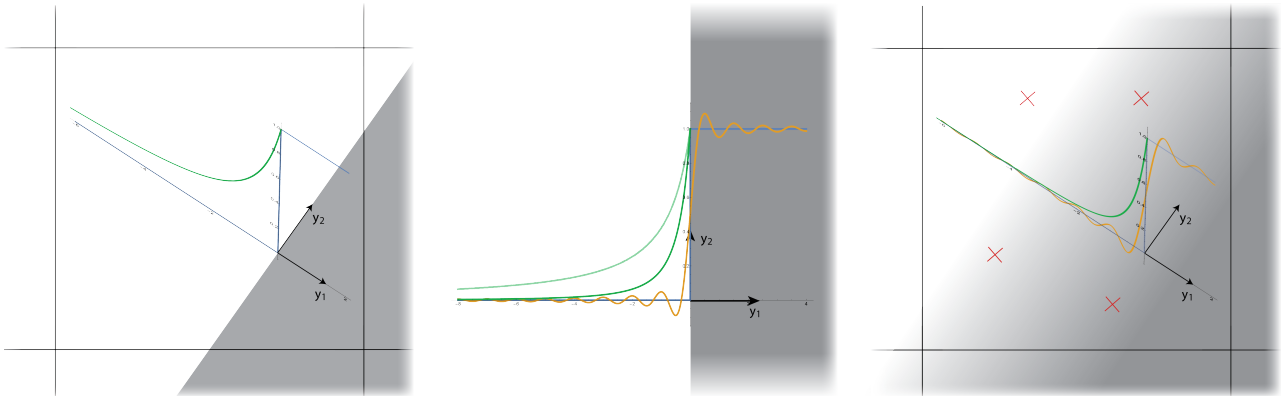

Figure 1: *Schematic depiction of our methodology.* Left: *Triangle (grey) partially covering a pixel. The (local) Fourier transform (green) of the jump discontinuity decays slowly, as* $1/|\xi|$*, only in the normal direction.* Middle: *After a change of coordinates the discontinuity is axis-aligned and the signal can be pre-filtered, resulting in much faster-decaying Fourier transform (dark green).* Right: *The pixel value can be computed efficiently from the pre-filtered signal using a sampling theorem adapted to the sampling locations and the pre-filtering.*

Eq. 6 is one example for such an expansion but many others exist. After inserting Eq. 7 into Eq. 1, the pixel value then is given by

$$I_{ij} = \int_{P_{ij}} \left(\sum_n I(\lambda_n)\, \tilde{k}_n(x) \right) dx = \sum_n I(\lambda_n) \int_{P_{ij}} \tilde{k}_n(x)\, dx \tag{8a}$$

and by computing

$$w_n = \int_{P_{ij}} \tilde{k}_n(x)\, dx \tag{8b}$$

we obtain the desired quadrature rule in Eq. 2. In practice, computing the w_k amounts to solving a linear system, see the supplementary material or [LDF14] for more details and background.

The above methodology will enable us to determine pixel values *when* the irradiance signal lies in a space $\mathcal{H}$ admitting a sampling theorem. However, in general this will not be the case. $I(x)$ then needs to be pre-filtered or regularized. This is accomplished by

$$\bar{I}(\bar{x}) = \int_{\mathbb{R}^2} I(x)\, k_{\bar{x}}(x)\, dx \tag{9}$$

where $k_{\bar{x}}(x)$ is the pointwise projection kernel that maps $I(x)$ onto $\mathcal{H}$; for B-bandlimited functions $k_{\bar{x}}(x) = \mathrm{sinc}(x - \bar{x})$ and one obtains the ideal pre-filtering for Shannon's theorem.

To simplify Eq. 9 we have to consider $I(x)$ in more detail. With the assumptions made in Sec. 1 we are interested in irradiance functions of the form $I(x) = t(x)\, H_{\vec{n}}(x)$ where $t(x)$ is the signal on the polygon, e.g. a texture, and $H_{\vec{n}}(x)$ is the Heaviside function with respect to the normal $\vec{n}$ of the jump discontinuity that is unity on the polygon and vanishes outside, see Fig. 1. Pre-filtering of textures has been studied extensively and can in practice be realized using mip-mapping. We will hence not consider it further and work in the following with $I(x) = H_{\vec{n}}(x)$, see Sec. 5 for a further discussion.

Since many spaces admitting sampling theorems, such as the space of B-bandlimited functions, can be described and analyzed efficiently in the frequency domain, it will be useful to also characterize $H_{\vec{n}}(x)$ using the Fourier transform. However, as is, the Fourier transform in Eq. 4 is defined over all of $\mathbb{R}^n$ and hence rather ill suited for analyzing a discontinuity in a small pixel neighborhood. Fortunately, the localization of the Fourier transform around a discontinuity has received considerable attention in mathematics and we can rely on the results obtained there, see e.g. [Ste93, Ch. VIII] or [Hör04, Vol. I]. In particular, if $f(x)$ is a discontinuous signal and $\phi(x)$ a smooth bump window in the vicinity of the jump, then for sufficiently larger $|\xi|$ the local Fourier transform $\widehat{(\phi f)}(\xi)$ decays slowly only for those directions $\bar{\xi} = \xi/|\xi|$ in Fourier space that correspond to a normal of the discontinuity. In the classical setting of B-bandlimited functions, this means that a discontinuous $f(x)$ is B-bandlimited for reasonably large B except when $\bar{\xi} = \vec{n}$. This observation that a discontinuous signal is ill-behaved only in the normal directions provides the conceptual underpinning for our approach.

To exploit the above result on the local Fourier transform of a discontinuity it is convenient to use a change of variables so that the jump is along a predetermined direction, say the x_1 axis. More concretely, we use a rotation $R_{\vec{n}}$ determined by the normal $\vec{n}$ so that $y = R_{\vec{n}} x$. Eq. 9 then becomes

$$\bar{H}'(y) = \int_{\mathbb{R}^2} H'(y)\, k'_{\bar{y}}(y)\, dy \tag{10}$$

where $H'(y) = H(R_{\vec{n}}^T y)$, cf. Fig. 1. The above integral is independent of the orientation and only one dimensional, since $H(R_{\vec{n}} x)$ is constant in the x_2 direction,

$$\bar{H}'(y) = \bar{H}'(y_1) = \int_{\mathbb{R}} H'(y_1)\, k'_{\bar{y}_1}(y_1)\, dy; \tag{11}$$

for simplicity we will identity H and H' in the sequel. As we will see in the following, the reduced Eq. 11 will enable us to determine an analytic solution or tabulate values for $\bar{H}(y_1)$. Importantly, the change of variables $y = R_{\vec{n}} x$ is compatible with the quadrature rule in Eq. 8. It becomes

$$I_{ij} = \sum_n w_n \bar{H}(R_{\vec{n}} \lambda_n)\,. \tag{12}$$

and at runtime it is thus sufficient to evaluate the pre-filtered signal $\bar{H}(y)$ at rotated sampling locations $R_{\vec{n}} \lambda_n$. In fact, since Eq. 11 is one dimensional the value of $\bar{H}(R_{\vec{n}} \lambda_n)$ only depends on the distance of λ_n to the discontinuity, which can also be computed directly.

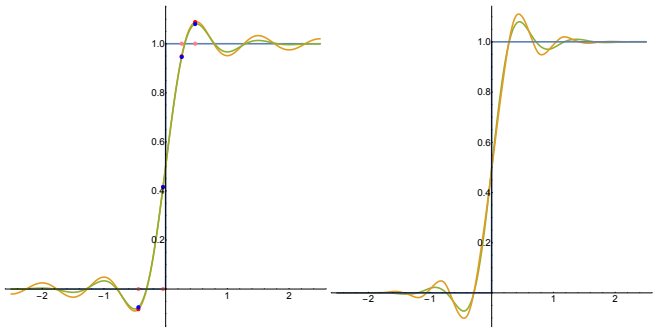

Figure 2: *Left: Step function $H(x)$ (light blue), its ideal 1-bandlimited version $Si_1(x)$, and $\mathrm{SCr}_{1,\beta}(x)$, i.e. the regularization of $H(x)$ obtained with the raised cosine. Also shown are four random samples in the vicinity of the jump for the different functions. Right: Ideal, $\bar{H}^a_4$, (orange) and faster decaying, $\bar{H}^{a,2}_4$, (green) regularized version of the step function $H(x)$ for Coiflets.*

In summary, our line of attack on visibility-induced aliasing will be to, first, choose a function space that admits a sampling theorem with respect to given λ_k, second, regularize the step function of the visibility discontinuity so that it lies in the space, third, use construct a sampling representation adapted to the space and the locations, and, fourth, derive quadrature weights from this representation. At runtime then only the quadrature rule in Eq. 12 needs to be evaluated.

3.3. Anti-aliasing in the Shannon-Nyquist setting

The classical setting for sampling is the space of B-bandlimited functions with the Shannon theorem in Eq. 6. Fixing this space we can apply the methodology developed in the last subsection.

Pre-filtering In the space of B-bandlimited functions the pre-filtering in Eq. 11 has a closed form solution given by

$$\bar{H}^i_B(x) = H(x) \star \mathrm{sinc}_B(x) = \frac{1}{\pi}\mathrm{Si}(2B\pi x) + \frac{1}{2} \tag{13}$$

where $\mathrm{Si}(x)$ is the sine integral

$$\mathrm{Si}(z) = \int_0^z \frac{\sin(x)}{x}\, dx; \tag{14}$$

numerically $\mathrm{Si}(x)$ can be evaluated efficiently using its Taylor expansion [RJM*15] (as other trigonometric functions).

As is well known, $\mathrm{Si}(x)$ suffers from ringing artifacts, see Fig. 2. These result from the discontinuities of the Fourier transform of the sinc-function, $\widehat{\mathrm{sinc}}(\xi) = \chi_B(\xi)$. The ringing can hence be reduced using a filter whose Fourier transform is more regular. A common choice is the raised cosine $\mathrm{Cr}_{B,\beta}(x)$ [PS08], see Fig. 3 for a depiction. The pre-filtering then still has a closed form solution,

$$\bar{H}^r_B(x) = H(x) \star \mathrm{Cr}_{B,\beta}(x) = \mathrm{SCr}(x) \tag{15}$$

where $\mathrm{SCr}(x)$ is provided in the supplementary material, see Fig. 2.

Construction of quadrature weights: equispaced samples The regularized jump discontinuities $\bar{H}^i_B(x)$ and $\bar{H}^r_B(x)$ in Eq. 13 and Eq. 15, respectively, are bandlimited and can hence be represented with equidistant samples using Shannon's theorem in Eq. 6. A quadrature rule can then be obtained as in Eq. 8 with the weights w_k being given by the integrals of the sinc-function over P_{ij}.

The Shannon theorem depends on infinitely many samples at all integers and, furthermore, through the non-compact support of the sinc-function, also all infinitely many weights w_k will be non-zero. Hence, also the quadrature rule will involve an infinite summation. To obtain a practical technique that can be implemented, and respect our assumptions from Sec. 1, we have to truncate the infinite sum to only involve samples in the pixel P_{ij}, i.e.

$$I_{ij} = \sum_{k \in P_{ij}} w_k \bar{I}_B(k/2B) + \sum_{k \in \mathbb{Z}^2 \setminus P_{ij}} w_k \bar{I}_B(k/2B) \tag{16}$$

with the second sum being set to zero. Unfortunately, the sinc-function decays only slowly as $1/|x|$ in the spatial domain so that the truncation will not provide a good approximation; see for example the paper by Strohmer and Tanner [ST05] for a rigorous bounds on the truncation error.

Construction of quadrature weights: non-equispaced samples In graphics, typically non-uniform samples are employed. Shannon's theorem is then no longer applicable. Within the space of B-bandlimited functions one can, however, construct generalizations for quite arbitrary locations [Beu66]. By the infinite support of the sinc-function the construction requires a priori the solution of an infinite-dimensional linear system to obtain the $\tilde{k}_n(x)$ (see the supplementary material). In practice, the system can be truncated in both dimensions and when Slepian functions are used this can be done with a very small error, see for example [XRY01]. The resulting reconstruction kernels $\tilde{k}_n(x)$ will, however, inherit the slow decay of the sinc-function, as follows from [Grö04, CG04, FG05], see Fig. 5 for an example. Hence, we have the same large truncation error as with the sinc-basis. We will thus turn next to a setting for sampling where faster-decaying reconstruction kernels are available.

3.4. Anti-aliasing using shift-invariant spaces

A family of function spaces that admit sampling theorems are shift-invariant spaces [AG01]. These are generated by generalizations of Eq. 6 where instead of the sinc-function one allows other, well-behaved kernels $\phi(x)$ that decays as $|x|$ increases. For fixed $\phi(x)$,

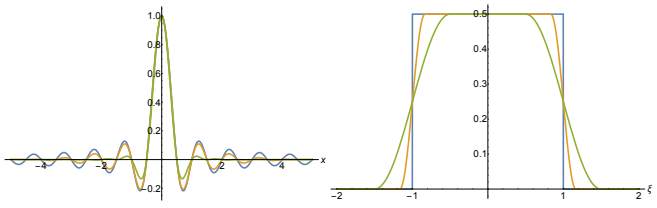

Figure 3: *Sinc function (blue) and raised cosine function in the spatial (left) and frequency (right) domains for different values of the parameter β that controls the localization (same colors correspond to the same value of β in both plots). Apparent is the much better spatial localization of the raised cosine function compared to the sinc-function at the cost of a less precise frequency localization.*

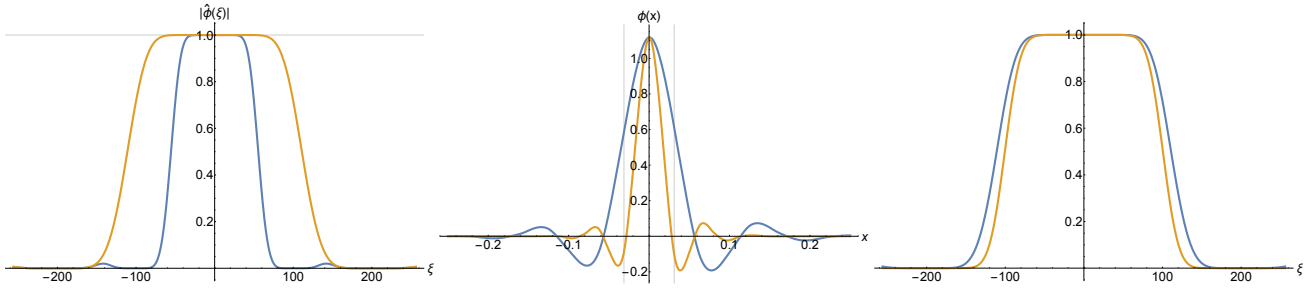

Figure 4: *Scaling function for Coiflet wavelets in the frequency (left) and spatial (middle) domain for dyadic dilations* 4 *and* 5. *It is apparent that the functions are very well localized in the spatial and frequency domains. The right plot shows a comparison of* $\hat{\phi}(\xi)$ *(blue) and* $|\hat{\phi}(\xi)|^2$ *(orange); it can be seen that* $\hat{\phi}(\xi)$ *decays smoother in the Fourier domain and will hence cause less ringing in the spatial domain when used as a regularization filter.*

the corresponding shift-invariant space is then defined as

$$\mathcal{H}^a_\phi = \left\{ f(x) = \sum_{k\in\mathbb{Z}^n} f_k \phi(ax-k) \mid f_k \in \ell_2 \right\}. \tag{17}$$

The dilation parameter a controls the "capacity" of the space, similar to the bandwidth B for the sinc-function.

A well known family of admissible kernels $\phi(x)$ are wavelet scaling functions with an associated multi-resolution analysis [Mal09, Ch. 3.1.3, Ch. 7.1]. These provide some additional advantages that make them a convenient choice for our purposes:

- dilation adjusts the effective frequency support;
- they form orthogonal bases; which simplifies the construction of sampling theorems and the computation of the coefficients f_k;
- they are compactly supported in space so that the corresponding dual reconstruction kernels $\tilde{k}_n(x)$ are also well localized;
- they are available in two dimensions.

To make the subsequent discussion more concrete, we will in the following employ the scaling function of the Coiflet wavelet of order 4, denoted as $\phi^a_4(x)$, with the associated space $\mathcal{H}^a_4$. This choice is motivated by the very good frequency localization of the function, see Fig.4, and because it has almost the sampling property [Mal09, Ch. 7.2.3].

Pre-filtering A simple approach for pre-filtering the step function $H(x)$ for $\mathcal{H}^a_4$ is obtained by considering the Fourier transform of $\phi^a_4(x)$, see Fig. 4. Since $\hat{\phi}^a_4(\xi)$ is a smoothed version of $\widehat{\mathrm{sinc}}(\xi) = \chi_B(\xi)$, not unlike the raised cosine, $\mathcal{H}^a_4$ is essentially the space of bandlimited functions for a bandlimit that is located before the transition region of $\hat{\phi}^a_4(\xi)$ begins (in fact, Daubechies constructed the functions such that this holds). This suggests that we can employ the regularized forms of $H(x)$ that were derived in the last section in Eq. 13 and Eq. 15 for the space of B-bandlimited functions. Among other things, these provide the advantage that they are given by closed form expressions.

The ideal pre-filtering for $\mathcal{H}^a_4$ is the orthogonal projection onto the space. Since the $\phi^a_4(x)$ form an orthonormal basis, it is given by

$$\bar{H}^a_4(x) = \sum_{k\in\mathbb{Z}^n} \left\langle H(y), \phi_4(ay-k) \right\rangle_y \phi_4(ax-k). \tag{18}$$

While no closed form solution exists for the inner product in the above equation, the required integrals can be computed to high accuracy using numerical quadrature. The resulting regularized step function is shown in Fig. 2.

Similar to the situation for B-bandlimited functions, the ideal $\bar{H}^a_4(x)$ in Eq. 18 suffers from ringing, although, because of the compact support of the $\phi^a_4(x)$, it is already much better localized than for $\mathrm{Si}(x)$. To understand how this ringing can be reduced, we consider Eq. 18 in the Fourier domain,

$$\hat{\bar{H}}_4(\xi) = \hat{H}(\xi) \left|\hat{\phi}^a_4(\xi)\right|^2. \tag{19}$$

Eq. 18 is thus equivalent to the convolution of $H(x)$ with the inverse Fourier transform of $\left|\hat{\phi}(\xi)\right|^2$. A filter that will result in less ringing should be smoother in the Fourier domain. Given the decay of $\left|\hat{\phi}(\xi)\right|^2$ from 1 to 0 as $|\xi|$ increases, see Fig. 4, one possible choice for a more regular filter is the "square root" of $\left|\hat{\phi}(\xi)\right|^2$. Conveniently, the "square root" is just the scaling function so that a spatial representation is available. The convolution

$$\bar{H}^{a,2}_4(x) = \phi^a_4(x) \star H(x) \tag{20}$$

cannot be computed analytically but an approximation to high accuracy is again possible numerically. We will refer to this approach as root pre-filtering in the following. A summary of the effect of different pre-filtering strategies is presented in Fig. 6.

Construction of Quadrature Weights The quadrature weights required to obtain $\tilde{I}_{ij}$ can again be derived as in Eq. 8 and are given by the integrals of the $\tilde{k}_n(x)$ over P_{ij}. Note that in contrast to the situation for the sinc-function computing the $\tilde{k}_n(x)$ only involves a finite dimensional linear system, since $\phi^a_4(x)$ is compactly supported.

Examples of reconstruction kernels $\tilde{k}_n(x)$ for the Coiflet setting are shown in Fig. 5 together with those obtained from the sinc-basis for the same sampling locations. Readily apparent is the much better localization of the $\tilde{k}_n(x)$ when one begins with a well-localized basis, as one would expect [Grö04, CG04, FG05].

3.5. What bandlimit should we use?

In the foregoing we assumed a fixed bandlimit B or a fixed dilation factor a. When the samples are equispaced the Nyquist condition and the spacing of the kernel function in Eq. 17, respectively, immediately answer how the parameters should be chosen. However,

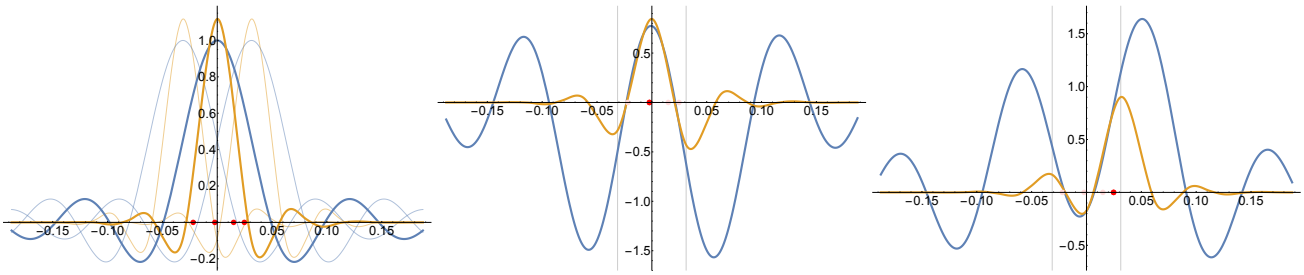

Figure 5: *Left: dilated, orthogonal basis functions at* $\{-1/32, 0, 1/32\}$ *for the sinc (blue) and Coiflet case (orange). Middle and right: dual kernel functions* $\tilde{k}(x)$ *for second and fourth sampling point (red) for the sinc (blue) and Coiflet case (orange) obtained with the three functions in the left plot; one readily sees that in the sinc-case* $\tilde{k}(x)$ *decays much slower than in the Coiflet-case, as expected from theory.*

for non-equispaced samples the correct choice is less obvious. Furthermore, we might have a number of samples, such as $m = 7$ or $m = 8$, that is not compatible with the tensor product structure of the bases where one always has $k^2, k \in \mathbb{Z}_+$, basis functions over a square domain. A conservative solution would be to use $k = \lfloor \sqrt{m} \rfloor$, resulting in $k^2 = 4$ for $m = 7$ or $m = 8$. However, this introduces an unnecessary error in the approximation $\tilde{H}$ and leads hence to a suboptimal pixel value. We are instead interested in choosing the largest possible space that is supported by the samples.

The problem of choosing B or a in the non-equispaced setting is dual to the question "How many non-uniform samples do we need?" for fixed B or a, which has been studied extensively in the literature. The answer is typically formulated using Beurling-type densities, see for example [Uns00, AG01, AS02] and references therein. Our answer for how to chose B and a will also rely on a density argument although we will remain less formal.

For concreteness let us consider the 8-point sample pattern that we will also employ in the next section, depicted as black dots in the inset figure. If we would have 9 samples then the largest possible tensor product space would be obtained by having the basis functions on a 3×3 grid over the pixel.

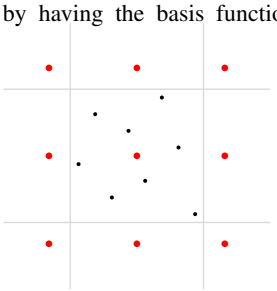

The given eight samples are, however, not enough for a locally 9-dimensional space and using a locally 4-dimensional one, with one basis function at each corner, is wasteful given the eight samples. To be able to choose an intermediate value, we introduce the local sample density, D_P, per pixel, which is similar to the notion of local dimensionality used before in graphics in [RMB07, LF10]. Assuming an image with N pixels in each direction parametrized over the unit square and basis functions at distance d, it is given by

$$D_P = \left(\frac{1}{N d} + 1 \right)^2 . \tag{21}$$

Given a local sample density, such as $D_P = 8$ in our case, we can solve the above equation for d which can then be related to the bandwidth $B = \pi/d$ and to the wavelet scale by $d = 2^{-l}$ with $a = 2^l$.

As an example, let $N = 16$. Then $d = 0.0342$, which is in between the sample spacing of $d = 1/16 = 0.0625$ for a locally 4-dimensional space and $d = 1/32 = 0.03125$ for a locally 9-dimensional space. The resulting basis function locations are shown in the inset figure (basis function locations in red).

4. Experiments

As examples, we applied the methodology proposed in the last section to the 4-sample and 8-sample antialiasing patterns used in DirectX 11.

To obtain experimental results we implemented a simple rasterizer for constant triangles in Mathematica. As reference solution we employed the exact area overlap of a triangle and a pixel and the reported classical pixel value is the unweighted average of the unfiltered signal. All numbers were obtained by averaging over a large number of randomly generated triangles and we verified that the numbers are consistent across multiple runs of the experiment. Our implementation is provided in the supplementary material.

4.1. 4-Sample Pattern

DirectX 4-sample pattern is a rotated, equi-distant grid. This substantially simplifies the construction since the bandlimit is obvious and the Shannon-theorem can be invoked directly using rotated sinc-functions. Since one has four samples, it is natural to employ

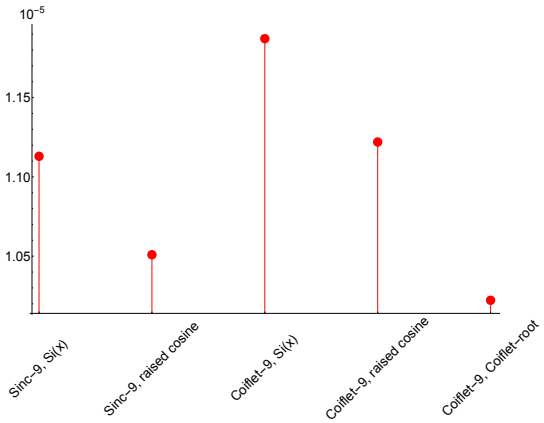

Figure 6: ℓ_2 *error for different pre-filtering for the 8-sample pattern. For all methods a weighted quadrature with the weights derived using Eq. 8 was employed.*

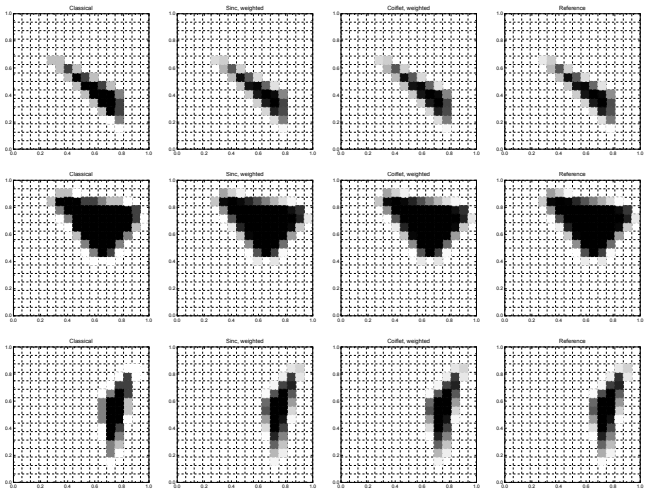

Figure 7: *Three triangles rasterized with pre-filtering and weighted quadrature for* 4 *samples per pixel. Even with four samples our results are visually almost indistinguishable from the ground truth.*

a locally 4-dimensional space for the Coiflet scaling functions with the functions located at the pixel corners, cf. Sec. 3.5. The various pre-filtering strategies introduced in Sec. 3 were used in the experiments and we also experimented with rotated, i.e. pixel boundary aligned filtering (reported as *-rot).

A depiction of the rasterization of some representative triangles with our approach is shown in Fig. 7. Already with four samples the obtained results are visually almost indistinguishable from the ground truth. Numerical results for the ℓ_p norms in Eq. 3 are reported in Fig. 8. These verify the visual impression of Fig. 7. Pre-filtering substantially reduces visibility-induced aliasing in all methods and even without quadrature weights (reported as 'MC') one obtains low error rates. The better localization of Coiflet scaling functions compared to the sinc-function further reduces the error rates in all error norms under consideration. The difference is not very pronounced but given the sample locations at hand that exactly fit the Shannon-Nyquist setting this is not entirely surprising. The results in Fig. 8 also demonstrate the benefits of using quadrature weights.

4.2. 8-Sample Pattern

For DirectX' 8-sample pattern we studied six different methods derived from our methodology. For Sinc-9 and Coiflet-9 we used nine basis functions and determined the bandlimit respectively the scale parameter using Eq. 21 and with one basis function located at the center of the pixel. The Sinc-4 case uses four sinc-functions centered in the pixel (i.e. the centroid of the four functions is the pixel center) with the same bandlimit as Sinc-9. We also explored locating our basis functions according to the Quincunx pattern (reported as *-Q. in the results). We again used the various pre-filtering strategies introduced in Sec. 3. A comparison is provided in Fig. 6.

Experimental results for the 8 sample case are presented in Fig. 9. Again, pre-filtering reduces the error for all methods and Coiflets provides a small but consistent advantage over the other techniques. That the ℓ_2 error is reduced is somewhat expected, since our approach is essentially developed in this setting. That also a significant reduction in the ℓ_∞ error is obtained is visually important since this norm is typically considered to be more closely related to perceptual results. Coiflet-9 and Sinc-9 significantly outperform the other methods which suggests that the notion of local dimensionality that we discussed in Sec. 3.5 is a suitable model.

5. Summary and Outlook

We demonstrated that visibility-induced aliasing can be reduced substantially by, first, choosing a suitable function space that admits a sampling theorem for the given locations; second, determining the pre-filtering of the step function for this space; third, constructing a sampling theorem with the given locations; and fourth, deriving the quadrature weights from the sampling theorem. We applied our methodology to the classical setting of bandlimited functions but also considered shift invariant spaces. We demonstrated that the better spatial localization of the kernel functions in the latter setting compared to the sinc-function also yields lower error rates.

We currently disregard textures, motivated by the fact that these can be pre-filtered efficiently using mip-mapping. However, since pre-filtering does not commute with multiplication of functions the interaction between the visibility discontinuity and textures requires further attention. Nonetheless, since a visibility event will only affect frequencies in the normal direction we do believe that our principal methodology is still applicable in the general case.

Our numerical experiments demonstrate the importance of quadrature weights for obtaining pixel values. We derived these from first principles, without the need to resort to optimization as in previous work [LA06]. In contrast to Laine and Aila [LA06], however, we did not take perceptual aspects into account. This is an important direction that should be explored in the future. Laine and Aila [LA06] also optimized sampling locations. Within our mathematical framework this has been explored previously by Lessig, Desbrun and Fiume [LDF14]. It will be interesting to incorporate it into the present work.

Our current methodology relies on polygonal edges being straight. This enabled us to reduce visibility anti-aliasing to a one dimensional problem along the direction where the Fourier transform decays slowly, that is the normal direction. For curved edges, such as in font outlines, our approach is hence not directly applicable. However, also for curved discontinuities is the local Fourier transform well understood [Ste93, Ch. VIII.5.B]. Roughly speaking, one then has slow decay for all directions in the normal cone of the neighborhood with the amount of Gaussian curvature controlling the constant of the decay. We believe that our approach is amenable to this setting using a non-linear coordinate transformation that straightens out the edge. Also the case of corners, where the Fourier transform decays slowly in all directions in the cone between adjacent normals [KP16] should be investigated in detail.

The setting considered in our work is closest to the rasterization pipeline and, unsurprisingly, it was developed with it in mind. Although our approach could probably be implemented using a combination of existing programmable shaders, we believe that it is best integrated into the rasterizer. Our methodology is, furthermore, not

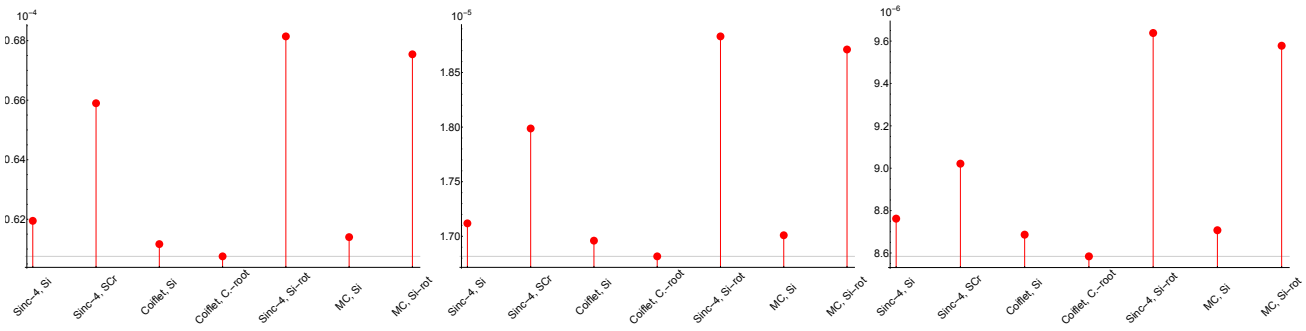

	Sinc-4, Si	Sinc-4, SCr	Coiflet, Si	Coiflet, root	Sinc-4, Si-rot	MC, Si	MC, Si-rot	Classical
$\ell_1 \times 10^{-5}$	6.19	6.59	6.12	6.08	6.81	6.14	6.75	28.4
ℓ_1, rel.	21.8%	23.2%	21.5%	21.4%	24.0%	21.6%	23.8%	100.0%
$\ell_2 \times 10^{-5}$	1.71	1.80	1.70	1.68	1.88	1.70	1.87	7.67
ℓ_2, rel.	22.3%	23.5%	22.1%	21.9%	24.6%	22.2%	24.4%	100.0%
$\ell_\infty \times 10^{-6}$	8.76	9.02	8.69	8.58	9.64	8.71	9.58	38.5
ℓ_∞, rel.	22.8%	23.4%	22.6%	22.3%	25.0%	22.6%	24.9%	100.0%

Figure 8: *4 samples: ℓ_1, ℓ_2, and ℓ_∞ errors (from left to right) and numerical results. For better visibility the data for the classical approach (not prefiltered, unweighted) has been excluded from the plots since it is five times larger than the remaining values, see the numerical data.*

restricted to rasterization and it will be interesting to adapt it to the image reconstruction pipeline used in ray tracers.

Acknowledgement

The present work was motivated by some questions by the NVIDIA research group on how to use insights from modern Fourier theory for practical pre-filtering. I would like to thank the NVIDIA research group for the opportunity to give a talk and for stimulating discussions. I also thank Clauson Carvalho da Silva for help with the closed form solution for the raised cosine pre-filter.

References

[AG01] ALDROUBI A., GRÖCHENIG K.: Nonuniform Sampling and Reconstruction in Shift-Invariant Spaces. *SIAM Review 43*, 4 (2001). 2, 4, 6

[AS02] ALDROUBI A., SUN Q.: Locally finite dimensional shift-invariant spaces in Rˆd. *Proceedings of the American Mathematical Society 130*, 9 (2002), 2641–2654. 6

[AW85] ABRAM G., WESTOVER L.: Efficient alias-free rendering using bit-masks and look-up tables. In *Proceedings of the 12th annual conference on Computer graphics and interactive techniques - SIGGRAPH '85* (New York, New York, USA, 1985), vol. 19, ACM Press, pp. 53–59. 2

[Beu66] BEURLING A.: Local harmonic analysis with some applications to differential operators. In *Some Recent Advances in the Basic Sciences, Proc. Annual Sci. Conf., Belfer Grad. School Sci., Yeshiva Univ* (New York, 1966), Belfer Graduate School of Science, Yeshiva Univ., New York, pp. 109–125. 4

[Cat78] CATMULL E.: A Hidden-Surface Algorithm with Anti-Aliasing. In *SIGGRAPH '78: Proceedings of the 5th annual conference on Computer graphics and interactive techniques* (New York, NY, USA, 1978), ACM, pp. 6–11. 1

[CG04] CORDERO E., GRÖCHENIG K.: Localization of frames II. *Applied and Computational Harmonic Analysis 17*, 1 (jul 2004), 29–47. 4, 5

[Coo86] COOK R. L.: Stochastic Sampling in Computer Graphics. *ACM Trans. Graph. 5* (1986), 51–72. 2

[Cro77] CROW F. C.: The Aliasing Problem in Computer-Generated Shaded Images. *Communications of the ACM 20* (1977), 799–805. 1

[DHS*05] DURAND F., HOLZSCHUCH N., SOLER C., CHAN E., SILLION F.: A Frequency Analysis of Light Transport. *ACM Transactions on Graphics (Proceedings of SIGGRAPH 2005) 24* (2005). 2

[DW85] DIPPÉ M. A. Z., WOLD E. H.: Antialiasing through Stochastic Sampling. In *SIGGRAPH '85: Proceedings of the 12th annual conference on computer graphics and interactive techniques* (New York, NY, USA, 1985), ACM, pp. 69–78. 2

[EHDR11] EGAN K., HECHT F., DURAND F., RAMAMOORTHI R.: Frequency Analysis and Sheared Filtering for Shadow Light Fields of Complex Occluders. *ACM Transactions on Graphics 30*, 2 (apr 2011), 1–13. 2

[FG05] FORNASIER M., GRÖCHENIG K.: Intrinsic Localization of Frames. *Constructive Approximation 22*, 3 (apr 2005), 395–415. 4, 5

[FLC80] FEIBUSH E. A., LEVOY M., COOK R. L.: Synthetic texturing using digital filters. In *Proceedings of the 7th annual conference on Computer graphics and interactive techniques - SIGGRAPH '80* (New York, New York, USA, 1980), vol. 14, ACM Press, pp. 294–301. 2

[Grö04] GRÖCHENIG K.: Localization of Frames, Banach Frames, and the Invertibility of the Frame Operator. *Journal of Fourier Analysis and Applications 10*, 2 (mar 2004), 105–132. 4, 5

[GT96] GUENTER B., TUMBLIN J.: Quadrature prefiltering for high quality antialiasing. *ACM Transactions on Graphics 15*, 4 (oct 1996), 332–353. 2

[Hec89] HECKBERT P.: *Fundamentals of Texture Mapping and Image Warping*. M.sc., University of California Berkeley, 1989. 1

[Hör04] HÖRMANDER L.: *The Analysis of Linear Partial Differential Operators*. Springer, 2004. 3

[KP16] KUTYNIOK G., PETERSEN P.: Classification of Edges Using Compactly Supported Shearlets. *Applied and Computational Harmonic Analysis* (nov 2016). 7

[LA06] LAINE S., AILA T.: A Weighted Error Metric and Optimization

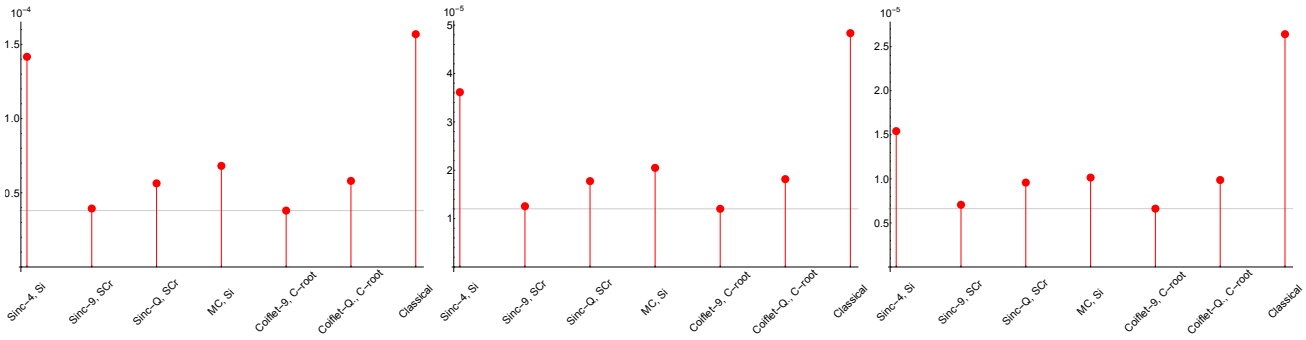

	Sinc-4, Si	Sinc-9, SCr	Sinc-Q, SCr	MC, Si	Coiflet-9, root	Coiflet-Q, root	Classical
$\ell_1 \times 10^{-5}$	14.	3.9	5.6	6.8	3.8	5.8	16.
ℓ_1, rel.	90.3%	25.1%	35.9%	43.4%	24.2%	37.0%	100.0%
$\ell_2 \times 10^{-5}$	3.6	1.3	1.8	2.0	1.2	1.8	4.8
ℓ_2, rel.	74.8%	26.0%	36.7%	42.4%	24.9%	37.6%	100.0%
$\ell_\infty \times 10^{-6}$	15.	7.1	9.6	10.	6.6	9.9	26.
ℓ_∞, rel.	58.3%	26.7%	36.3%	38.4%	25.1%	37.4%	100.0%

Figure 9: *8 samples: ℓ_1, ℓ_2, and ℓ_∞ errors (from left to right) and numerical results.*

Method for Antialiasing Patterns. *Computer Graphics Forum 25*, 1 (mar 2006), 83–94. 1, 2, 7

[LDF14] LESSIG C., DESBRUN M., FIUME E.: A Constructive Theory of Sampling for Image Synthesis Using Reproducing Kernel Bases. *ACM Transactions on Graphics (Proceedings of SIGGRAPH 2014) 33*, 4 (jul 2014), 1–14. 2, 3, 7

[LF10] LESSIG C., FIUME E.: On the Effective Dimension of Light Transport. *Computer Graphics Forum (Proceedings of EGSR 2010) 29*, 4 (aug 2010), 1399–1403. 6

[Mal09] MALLAT S. G.: *A Wavelet Tour of Signal Processing: The Sparse Way*, third ed. ed. Academic Press, 2009. 5

[McC95] MCCOOL M. D.: Analytic antialiasing with prism splines. In *Proceedings of the 22nd annual conference on Computer graphics and interactive techniques - SIGGRAPH '95* (New York, New York, USA, 1995), ACM Press, pp. 429–436. 2

[Mit87] MITCHELL D. P.: Generating Antialiased Images at Low Sampling Densities. In *SIGGRAPH '87: Proceedings of the 14th annual conference on Computer graphics and interactive techniques* (New York, NY, USA, 1987), ACM, pp. 65–72. 2

[Mit91] MITCHELL D. P.: Spectrally Optimal Sampling for Distribution Ray Tracing. *SIGGRAPH Comput. Graph. 25* (1991), 157–164. 2

[MN88] MITCHELL D. P., NETRAVALI A. N.: Reconstruction Filters in Computer-Graphics. *ACM SIGGRAPH Computer Graphics 22*, 4 (aug 1988), 221–228. 2

[MS13] MANSON J., SCHAEFER S.: Analytic Rasterization of Curves with Polynomial Filters. *Computer Graphics Forum 32*, 2-4 (may 2013), 499–507. 2

[OF01] OUELLETTE M. J., FIUME E.: On Numerical Solutions to One-Dimensional Integration Problems with Applications to Linear Light Sources. *ACM Trans. Graph. 20* (2001), 232–279. 2

[PS08] PROAKIS J. G., SALEHI M.: *Digital Communications*. McGraw-Hill, 2008. 4

[RAMN12] RAMAMOORTHI R., ANDERSON J., MEYER M., NOWROUZEZAHRAI D.: A Theory of Monte Carlo Visibility Sampling. *ACM Transactions on Graphics 31*, 5 (aug 2012), 1–16. 2

[Res09] RESHETOV A.: Morphological Antialiasing. In *Proceedings of the 1st ACM conference on High Performance Graphics - HPG '09* (New York, New York, USA, 2009), ACM Press, p. 109. 1, 2

[RJM*15] ROWE B. T. P., JARVIS M., MANDELBAUM R., BERNSTEIN G. M., BOSCH J., SIMET M., MEYERS J. E., KACPRZAK T., NAKAJIMA R., ZUNTZ J., MIYATAKE H., DIETRICH J. P., ARMSTRONG R., MELCHIOR P., GILL M. S. S.: GalSim: The modular galaxy image simulation toolkit. *Astronomy and Computing 10* (apr 2015), 121–150. 4

[RKLC*11] RAGAN-KELLEY J., LEHTINEN J., CHEN J., DOGGETT M., DURAND F.: Decoupled Sampling for Graphics Pipelines. *ACM Transactions on Graphics 30*, 3 (may 2011), 1–17. 1

[RMB07] RAMAMOORTHI R., MAHAJAN D., BELHUMEUR P.: A First-Order Analysis of Lighting, Shading, and Shadows. *ACM Trans. Graph. 26* (2007), 2. 6

[ST05] STROHMER T., TANNER J.: Implementations of Shannon's sampling theorem, a time-frequency approach. *Sampling Theory in Signal and Image Processing 4*, 1 (2005), 1–17. 4

[Ste93] STEIN E. M.: *Harmonic Analysis: Real-Variable Methods, Orthogonality, and Oscillatory Integrals*. Princeton Mathematical Series. Princeton University Press, Princeton, 1993. 3, 7

[Uns00] UNSER M.: Sampling—50 Years After Shannon. *Proceedings of the IEEE 88* (apr 2000), 569–587. 6

[Wil83] WILLIAMS L.: Pyramidal parametrics. In *Proceedings of the 10th annual conference on Computer graphics and interactive techniques - SIGGRAPH '83* (New York, New York, USA, 1983), vol. 17, ACM Press, pp. 1–11. 1

[XRY01] XIAO H., ROKHLIN V., YARVIN N.: Prolate spheroidal wavefunctions, quadrature and interpolation. *Inverse Problems 17*, 4 (2001), 805–838. 4

[ZJL*15] ZWICKER M., JAROSZ W., LEHTINEN J., MOON B., RAMAMOORTHI R., ROUSSELLE F., SEN P., SOLER C., YOON S.-E.: Recent Advances in Adaptive Sampling and Reconstruction for Monte Carlo Rendering. *Computer Graphics Forum 34*, 2 (may 2015), 667–681. 2